Available online at www.sciencedirect.com
ScienceDirect
Journal of Power Sources 179 (2008) 60–68
JOURNAL OF POWER SOURCES
www.elsevier.com/locate/jpowsour

Properties and performance of $Ba_{0.5}Sr_{0.5}Co_{0.8}Fe_{0.2}O_{3-\delta}$ + $Sm_{0.2}Ce_{0.8}O_{1.9}$ composite cathode

Kang Wang [a], Ran Ran [a], Wei Zhou [a], Hongxia Gu [a], Zongping Shao [a,*], Jeongmin Ahn [b]

[a] *State Key Laboratory of Materials-Oriented Chemical Engineering, Nanjing University of Technology, Xin Mofan Road, Nanjing, JiangSu 210009, PR China*
[b] *School of Mechanical and Materials Engineering, Washington State University, Sloan 217, Pullman, WA 99164-2920, USA*

Received 7 November 2007; received in revised form 13 December 2007; accepted 13 December 2007
Available online 1 February 2008

Abstract

The properties and performance of $Ba_{0.5}Sr_{0.5}Co_{0.8}Fe_{0.2}O_{3-\delta}$ (BSCF) + $Sm_{0.2}Ce_{0.8}O_{1.9}$ (SDC) (70:30 in weight ratio) composite cathode for intermediate-temperature solid-oxide fuel cells were investigated. Mechanical mixing of BSCF with SDC resulted in the adhesion of fine SDC particles to the surface of coarse BSCF grains. XRD, SEM-EDX and O_2-TPD results demonstrated that the phase reaction between BSCF and SDC was negligible, constricted only at the BSCF and SDC interface, and throughout the entire cathode with the formation of new (Ba,Sr,Sm,Ce)(Co,Fe)$O_{3-\delta}$ perovskite phase at a firing temperature of 900, 1000, and $\geq$ 1050 °C, respectively. The BSCF + SDC electrode sintered at 1000 °C showed an area specific resistance of ~0.064 Ω cm^2 at 600 °C, which is a slight improvement over the BSCF (0.099 Ω cm^2) owing to the enlarged cathode surface area contributed from the fine SDC particles. A peak power density of 1050 and ~382 mW cm^{-2} was reached at 600 and 500 °C, respectively, for a thin-film electrolyte cell with the BSCF + SDC cathode fired from 1000 °C.

Keywords: $Ba_{0.5}Sr_{0.5}Co_{0.8}Fe_{0.2}O_{3-\delta}$; Samaria doped ceria; Solid-oxide fuel cells; Cathode

1. Introduction

Solid-oxide fuel cells (SOFCs) are all-solid electrochemical devices that convert the chemical energy stored in fuels to electricity in a highly efficient and low-emission way. Recently, SOFCs have received considerable attention due to the increased importance of sustainability associated with future worldwide development [1–3].

The solid-state reaction between the electrolyte and electrode is a practical problem, since such a reaction could occur during the fabrication and application of SOFCs [4–8]. The reaction may result in the formation of non-conducting phases between the electrode and electrolyte interface, which would greatly increase the interfacial polarization resistance of the cathode. On the other hand, the electrocatalyst-electrolyte composite cathode is frequently applied in an attempt to improve the performance of oxide electrodes [9–13]. However, the phase reaction between the components in the composite electrode and its influence on the cathode performance has been rarely exploited [14,15].

$Ba_{0.5}Sr_{0.5}Co_{0.8}Fe_{0.2}O_{3-\delta}$ (BSCF) is a promising cathode material for intermediate-temperature (IT) SOFCs [16–19]. The BSCF + SDC (samaria doped ceria) composite has also been investigated as a potential cathode for IT-SOFCs [20–22]. Detailed and systematical investigations into the reaction mechanism between BSCF and SDC are helpful in order to optimize the BSCF + SDC cathode. These investigations are also important in that they serve as guidance for the development of new composite cathode materials.

In this study, the performance of the BSCF + SDC composite cathode was intensely examined. Particular attention was paid to the phase reaction between BSCF and SDC and its effect

* Corresponding author. Tel.: +86 25 83587722; fax: +86 25 83365813.
E-mail address: shaozp@njut.edu.cn (Z. Shao).

0378-7753/$ – see front matter © 2008 Elsevier B.V. All rights reserved.
doi:10.1016/j.jpowsour.2007.12.051

on the performance of the composite cathode at intermediate temperatures.

2. Experimental

2.1. Powder synthesis

BSCF and SDC powders were prepared by a combined EDTA-citrate complexing method [23]. Metal nitrates in analytic grade were made into aqueous solutions. Their precise concentrations were determined by the EDTA titration method. These metal nitrates were then used as the metal ion sources. The required amounts of metal nitrates were set according to the stoichiometry of the aimed product. They were made into a mixed aqueous solution, followed by the addition of EDTA and citric acid, where both served as complexing agents to ensure the molecule-level homogeneous mixing of the metal ions in the solution. NH_4OH was applied during the evaporation process to ensure a solution pH value of ~6. Through heating and stirring, a clear gel was finally obtained. The gel was then heated at 250 °C for 10 h to form a solid precursor and finally calcined at 900 °C for 5 h to result in oxides with the desired final composition and lattice structure.

2.2. Material characterization

The phase structure of the oxide samples from various conditions was observed through the use of an X-ray diffractometer (XRD, Bruker D8 Advance). The microscopic features of the prepared electrodes were characterized using an Environmental Scanning Electron Microscope (ESEM, QUATA-2000) equipped with an Energy-Dispersive X-ray (EDX) attachment. The specific surface areas of the samples were characterized by N_2 adsorption using a BELSORP II instrument at the temperature of liquid nitrogen. Electrical conductivity was measured within the temperature range of 300–900 °C at intervals of 10 °C by using the four-terminal DC technique over bar-shape samples with dimensions of $2 \times 5 \times 12\,mm^3$, and Ag paste was used for electrodes. Current and voltage were applied/detected by the Keithely 2420 source meter. Sufficient stabilization time was applied at each measurement point in order to ensure that the electrical conductivity reached steady state.

Under the reduced atmosphere (inert gas) and with the programmed increase of the temperature, the metal ions in oxides with variable valence states could be thermally reduced. The reduction process results in the release of lattice oxygen, which can be detected by a mass spectrometer or gas chromatography. Such a process is denoted as O_2-TPD thereafter. For a typical O_2-TPD experiment in this study, about 150 mg sample was loaded into a U-type quartz glass tube with an inner diameter of 1 mm. The reactor was then placed in a single-zone furnace equipped with a temperature controller. Argon was used as the carrier gas at a flow rate of $20\,ml\,min^{-1}$. The temperature was increased from 200 to 1000 °C at a rate of $10\,°C\,min^{-1}$. The effluent gases were monitored by a mass spectrometer (Hiden, QIC-20).

2.3. Symmetric cell and fuel cell fabrication

Symmetric cells with the configuration of electrode |SDC|electrode were applied for the impedance studies. Dense SDC pellets of 12 mm in diameter and 0.8 mm in thickness were prepared by dry pressing and then were sintered in air at 1350 °C for 5 h. To prepare the composite electrode, the BSCF and SDC powders with the weight ratio of 70:30 were first dispersed in a pre-mixed solution of glycerol, ethylene glycol and isopropyl alcohol to form a colloidal suspension by utilizing a high-energy ball milling process. The resultant colloidal suspension was then spray deposited symmetrically on both surfaces of the SDC pellet using a spray gun with N_2 as the carrier gas, and then calcined at 900–1100 °C for 5 h in ambient air to form the porous symmetric electrode layers.

Anode-supported complete cells with the SDC electrolyte were prepared using a co-pressing technique. Anode powders consisting of 60 wt.% NiO and 40 wt.% SDC were prepared by mixing NiO and SDC physically in an agate mortar by hand. To fabricate the single cell, the well-mixed NiO + SDC powders were first pressed as substrates; SDC powders were then added onto the substrates and pressed again to form bi-layer pellets (area: $\sim 1.25\,cm^2$), which were fired in air at 1450 °C for 5 h in order to achieve the densification of the electrolyte layer. The BSCF + SDC colloidal suspension was then spray deposited onto the electrolyte surfaces of the sintered bi-layer pellets, and then fired at 1000 °C for 5 h to form the compete cells with a porous cathode layer (area: $\sim 0.48\,cm^2$).

2.4. Electrochemical performance test

The electrode performance was investigated with a symmetrical or complete cell configuration by the AC impedance method using an electrochemical workstation composed of a Solartron 1287 potentiostat in combination with a 1260A frequency response analyzer. The applied frequency ranged from 0.01 Hz to 100 kHz with a signal amplitude of 10 mV under open circuit voltage (OCV) conditions. The overall impedance data were fitted by a complex non-linear least squares (CNLS) fitting program in ZView 2.9b software. *I–V* polarization curves were collected using a Keithley 2420 source meter based on the four-terminal configuration. The fuel cell was sealed onto a quartz tube reactor with the cathode side exposed to ambient air. Pure hydrogen at a flow rate of $80\,ml\,min^{-1}$ [STP] was fed into the anode chamber as fuel. Silver paste was painted over the electrode surface as the current collector by a brush and the cell with the current collector was fired at 800 °C for half an hour before the test.

3. Results and discussion

3.1. Effect of firing temperature on the phase reaction between SDC and BSCF

It is well known that cobalt-based perovskite materials have high reactivity. The reaction between cobalt-contained BSCF and SDC at various firing temperatures were investigated by ex-

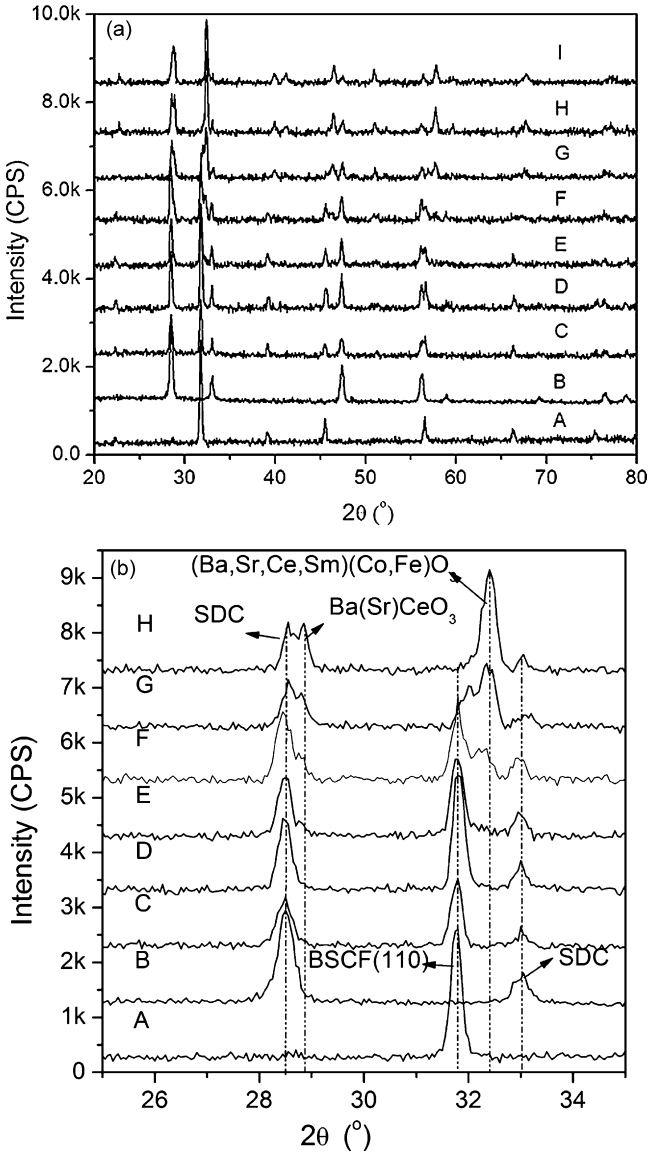

Fig. 1. (a) X-ray diffraction patterns of (A) 900 °C calcined SDC; (B) 900 °C calcined BSCF; (C) fresh mechanically mixed BSCF + SDC composite; (D, E, F, G, H) sample C further calcined/fired at 900, 950, 1000, 1050 and 1100 °C for 5 h under air, respectively; (I) sol–gel derived BSCF + SDC composite and (b) magnified XRD patterns from 25° to 35°.

situ techniques. BSCF and SDC were mechanically mixed at the weight ratio of 70:30 with the help of a high-energy ball miller (Fritsch Pulverisette 6) employing zirconium oxide as the grinding ball and isopropyl alcohol as the solvent, and then calcined at various temperatures in air for 5 h. 900 °C calcined BSCF and SDC from an EDTA–citrate complexing process were applied as the starting materials for this study. After the calcination, the samples were cooled to room temperature and examined by various techniques to detect the possible phase reaction. Fig. 1 shows the X-ray diffraction patterns of the BSCF + SDC composite oxides that were calcined at various temperatures for 5 h. For comparison, the patterns of the 900 °C calcined BSCF and SDC samples were also presented. As can be seen, the raw materials of the BSCF and SDC show the pure cubic perovskite phase and cubic fluorite phase, respectively. The BSCF + SDC after being calcined at 900 °C for 5 h showed similar diffraction patterns to the non-calcined mixture. This suggests that the phase reaction between the BSCF and SDC at 900 °C was negligible. When the calcination temperature was elevated to 1000 °C, additional diffraction peaks appeared, located near the right side of the main BSCF peak, suggesting the formation of a new perovskite oxide (perovskite-B) with a smaller lattice parameter to BSCF. Furthermore, a new diffraction peak appeared at 2θ of 28.8°, which was ascribed to the $Ba(Sr)CeO_3$ phase (Fig. 1(b)). With the further increase of calcination/firing temperature, the intensity of the BSCF and SDC diffraction peaks decreased while the intensity of perovskite-B increased. When the calcination temperature was increased to 1100 °C, the BSCF phase completely disappeared while the intensity of perovskite-B phase was obviously strengthened.

The final reaction products of BSCF and SDC were examined by sol–gel synthesis based on the EDTA–citrate complexing process. Metal nitrates of $Ba(NO_3)_2$, $Sr(NO_3)_2$, $Co(NO_3)_2$, $Fe(NO_3)_3$, $Sm(NO_3)_3$ and $Ce(NO_3)_3$ according to the stoichiometry of BSCF + SDC (70:30 in weight ratio) composite were mixed in the solution stage of the EDTA–citrate complexing process. The metal diffusion block was eliminated during the phase formation. Therefore, the obtained products reflect the most stable products of the solid-state reaction between BSCF and SDC. Such a sample was named as sol–gel derived BSCF + SDC composite in the following section of this paper. As shown in Fig. 1, it had the same diffraction patterns as the 1100 °C calcined mechanically mixed BSCF + SDC composite. This suggests that the solid-state reaction between BSCF and SDC was completed at 1100 °C.

It is well known that samaria and ceria both can dope into the A-site of the perovskite, and the successful doping of ceria into the B-site of perovskite has also been reported [24–29]. Ce^{3+} and Sm^{3+} have smaller ionic radii than Ba^{2+} and Sr^{2+}, and their doping into the A-site of BSCF would result in the shrinking of the lattice. While Ce^{4+} has a much larger ionic radius (0.87 Å) than cobalt (HS (high spin)-Co^{2+}: 0.745 Å; HS–Co^{3+}: 0.61 Å, HS–Co^{4+}: 0.53 Å) and iron (HS–Fe^{3+}:0.645 Å, Fe^{4+}: 0.585 Å) at the B-site, the doping of ceria into the B-site would result in the expansion of the lattice. Since a smaller lattice parameter for the perovskite-B than the BSCF was observed, samaria and ceria were likely incorporated into the A-site of the BSCF during the firing process. This assumption is supported by the successful synthesis of the perovskite oxides with the desired compositions of $(Ba_{0.5}Sr_{0.5})_{0.8}Sm_{0.2}Co_{0.8}Fe_{0.2}O_{3-\delta}$, $(Ba_{0.5}Sr_{0.5})_{0.8}Ce_{0.2}Co_{0.8}Fe_{0.2}O_{3-\delta}$ and $(Ba_{0.5}Sr_{0.5})_{0.8}(Sm_{0.2}Ce_{0.8})_{0.2}Co_{0.8}Fe_{0.2}O_{3-\delta}$ based on an EDTA–citrate complexing process as shown in Fig. 2.

Fig. 3 shows the surface morphologies of BSCF, SDC and BSCF + SDC (70:30 in weight ratio) mixed powders fired at various temperatures for 5 h. The BSCF oxide had a grain size of 1–5 μm, while the SDC had a finer particle size of ~100 nm. BET measurements show that the BSCF had a surface area of only 0.25–0.4 $m^2\,g^{-1}$ and the SDC of ~6 $m^2\,g^{-1}$ (1000 °C calcined). Fig. 3C shows the typical morphologies of the very fine particles surrounding the surface of the BSCF with a larger grain size in the non-calcined mechanically mixed BSCF + SDC

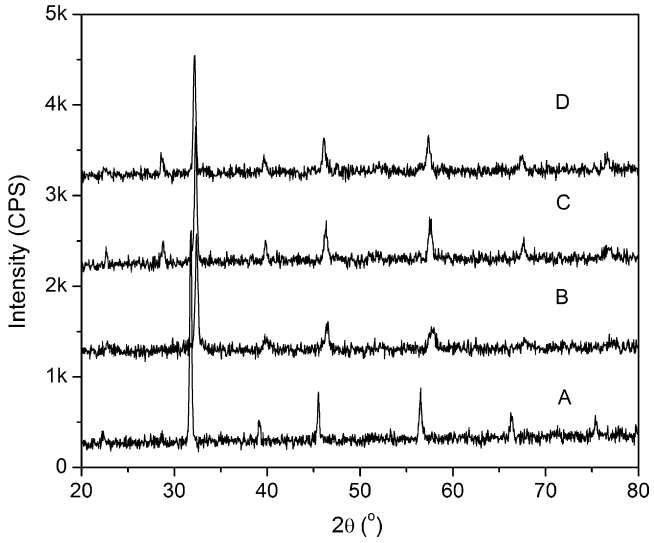

Fig. 2. X-ray diffraction patterns of (A) BSCF; (B) $Sm_{0.2}(Ba_{0.5}Sr_{0.5})_{0.8}Co_{0.8}Fe_{0.2}O_{3-\delta}$; (C) $Ce_{0.2}(Ba_{0.5}Sr_{0.5})_{0.8}Co_{0.8}Fe_{0.2}O_{3-\delta}$; (D) $(Sm_{0.8}Ce_{0.2})_{0.2}(Ba_{0.5}Sr_{0.5})_{0.8}Co_{0.8}Fe_{0.2}O_{3-\delta}$.

powders. Similar phenomena were also observed in the investigation of the BSCF + $LaCoO_3$ composite cathode [30]. When the mixed powders were calcined at 1000 °C for 5 h (Fig. 3D), the SDC grains grew obviously as compared with the fresh samples. Based on the EDX results, at least two micro domains i.e., the BSCF-enriched phase and the SDC-enriched phase, were observed. The adhesion of SDC to BSCF was much improved after the calcination. However, the (Ba,Sr,Ce,Sm)(Co,Fe)$O_{3-\delta}$ was hardly detected by SEM-EDX for this sample. From the combined SEM-EDX and XRD results, it is proposed that the formation of the new phase was located only at the BSCF–SDC interface. With the further increase of the calcination temperature to 1100 °C, the BSCF phase completely disappeared. The only observable phase by EDX was (Ba,Sr,Ce,Sm)(Co,Fe)$O_{3-\delta}$ perovskite, which was well sintered as shown in Fig. 3E.

The phase reaction between the BSCF and SDC was further investigated by the O_2-TPD technique. For the perovskite under programmed heating in a reduced oxygen partial pressure atmosphere (argon), the B-site metal ions with variable valence states is thermally reduced to lower valence states accompanied with the release of oxygen from the lattice structure. The released oxygen can be in-situ detected by a mass spectrometer. Normally, two types of desorption peaks may be observed for cobalt and iron based perovskites. For such perovskites, one or more peaks between 300 and 600 °C are associated with the reduction of Co^{4+}/Fe^{4+} to Co^{3+}/Fe^{3+}. Sometimes one or more additional peaks may be observed at $T > 700$ °C, and this is related to the thermal reduction of Co^{3+} to Co^{2+}. The shape and position of the peaks are closely related with the elemental composition in the A and B-sites of perovskite. The different metal ions in the A-site of perovskite affect the reduction/oxidation properties of the B-site metal ions. The shift of the oxygen desorption peak reflects the compositional change of the perovskite. Fig. 4 shows the O_2-TPD profiles of BSCF, sol–gel derived BSCF + SDC composite, and mechanically mixed BSCF + SDC mixture calcined at various temperatures for 5 h (25, 900, 950, 1000, 1050 and 1100 °C). The BSCF sample showed only one desorption peak (peak-A) at around 410 °C at the low temperature zone (300–600 °C). For the sol–gel derived BSCF + SDC composite, one desorption peak (peak-B) was also present, but shifted slightly to a lower temperature of ~360 °C. Based on the XRD and SEM-EDX results, the sol–gel derived BSCF + SDC composite was mainly composed of (Ba,Sr,Ce,Sm)(Co,Fe)$O_{3-\delta}$ perovskite. Therefore, peak-B was assigned to the release of oxygen from the lattice of the (Ba,Sr,Ce,Sm)(Co,Fe)$O_{3-\delta}$ phase. This suggests that the incorporation of Sm^{3+} and Ce^{3+} into the A-site of the BSCF resulted in the increased reducibility of cobalt and iron ions in the perovskite. For the sample calcined at 900 °C, only one desorption peak around 410 °C was observed, which was located at the same position as that of the non-calcined mechanically mixed BSCF + SDC oxides and the pure BSCF. This suggests that the reaction between the BSCF and SDC was negligible at 900 °C, which agrees well with the XRD results. At a calcination temperature of 950 °C, the desorption peak shifted slightly to a lower temperature of 390 °C. With the further increase of the calcination temperature to 1000 °C, two strongly overlapped desorption peaks were observed with the new appearance of one (peak-B) located near the peak-A. This suggests that a partial reaction between the BSCF and SDC with the formation of (Ba,Sr,Ce,Sm)(Co,Fe)$O_{3-\delta}$ phase occurred, and this coincides well with the XRD results. The intensity of peak-B increased steadily with temperature while it decreased for peak-A. Only peak-B survived after calcination at 1050 °C or higher, suggesting the complete reaction of BSCF and SDC. The aforementioned conclusions were also in agreement with those derived based on X-ray and SEM-EDX results.

3.2. *Influence of phase reaction on the electrochemical performance of BSCF + SDC*

As demonstrated previously, the phase reaction between BSCF and SDC is closely related with the firing temperatures. The effect of phase reaction on the cathode performance was then indirectly examined by varying the firing temperatures for the cathode layer. The area specific resistances (ASRs) of the BSCF + SDC electrode fired at various temperatures are presented in Fig. 5. The ASR experienced a decrease with temperature that reached a minimum value at 1000 °C, and then increased sharply with the further increase of firing temperature. For example, the ASR of the cathodes at 600 °C fired from 900, 950, 1000, 1050 and 1100 °C, was 0.184, 0.106, 0.064, 0.176 and 0.270 $\Omega\,cm^2$, respectively. A similar trend was also observed for the SSC + SDC cathode in literature [31].

The BSCF + SDC demonstrated modestly better performance than the BSCF cathode when the firing temperature was 1000 °C. However, it showed a worse performance than the BSCF at other temperatures. Even when fired at 1000 °C, the increase in cathode performance with the SDC addition was very limited for the BSCF + SDC cathode. For example, an ASR of about 0.099 $\Omega\,cm^2$ was observed for a pure BSCF cathode, while it was about 0.064 $\Omega\,cm^2$ for a BSCF + SDC composite cathode with an improvement of only ~36%. For SSC, LSM and LSCF, the formation of a composite cathode by the introduction of

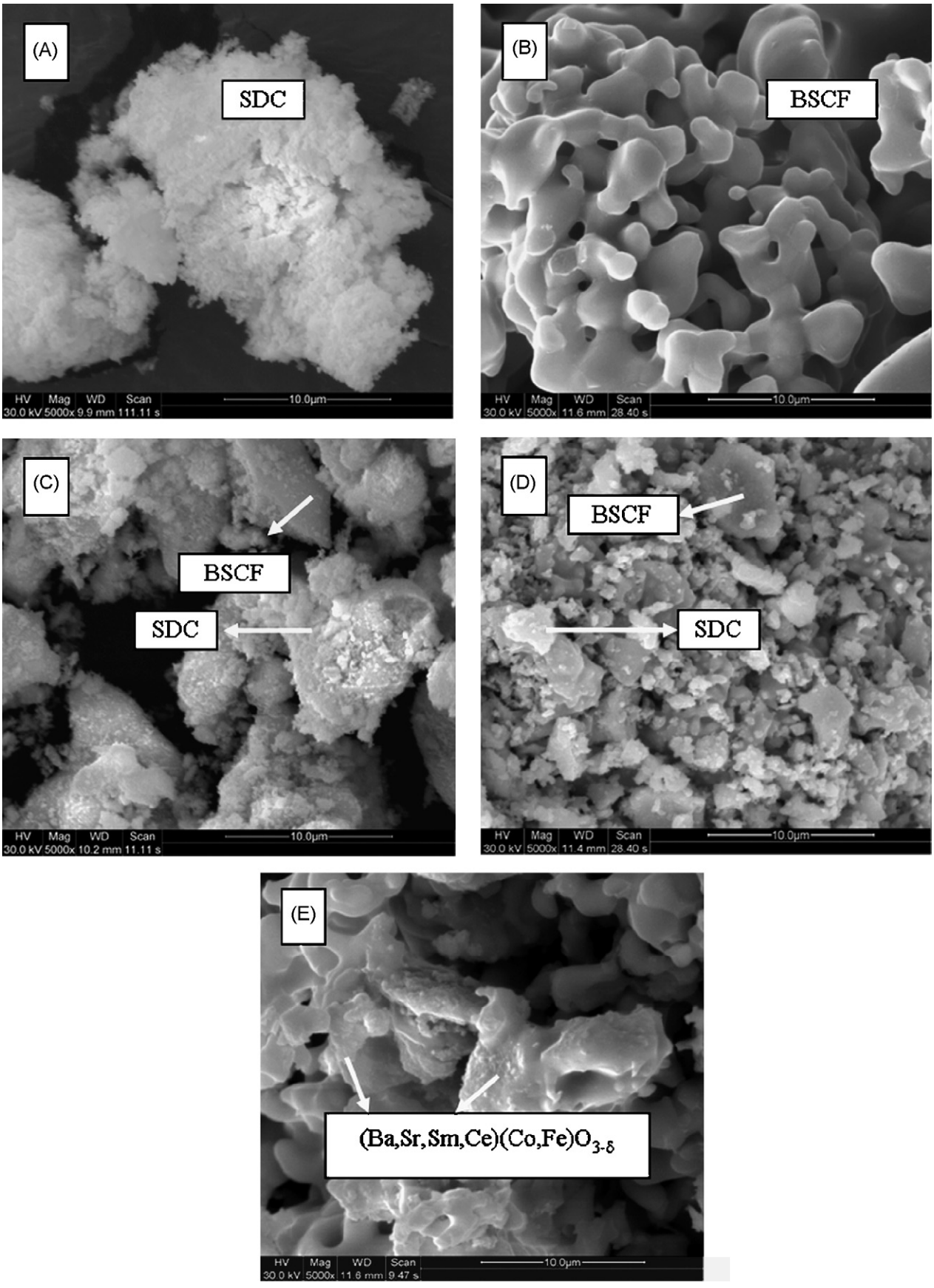

Fig. 3. SEM morphologies of (A) SDC; (B) BSCF; (C–E) mechanically mixed BSCF + SDC composite (70:30 in weight ratio) with (C) before calcinations; (D) calcined at 1000 °C for 5 h; and (E) calcined at 1100 °C for 5 h.

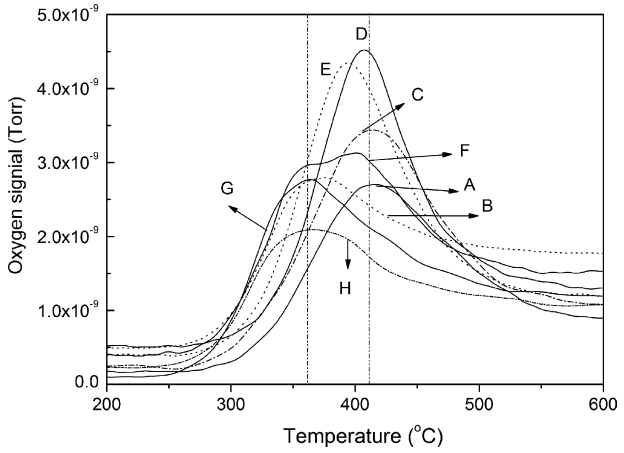

Fig. 4. O_2-TPD profiles of (A) pure BSCF; (B) sol–gel derived BSCF + SDC composite; (C, D, E, F, G) and (H) mechanically mixed BSCF + SDC composite calcined/fired at 900, 950, 1000, 1050 and 1100 °C for 5 h under air, respectively.

ionic conducting phase resulted in the improvement of the cathode performance by more than one order of magnitude [31–33]. Such improvement was due to the extension of the active oxygen reduction sites from the traditional electrode–electrolyte–gas phase (three-phase-boundary, TPB) to the entire cathode layer. Since the BSCF by itself is a mixed conducting oxide with the oxygen ionic conductivity even higher than SDC [16], the slightly better performance for the BSCF + SDC cathode as compared with the pure BSCF was unlikely contributed from the oxygen ionic conductivity of SDC. Based on the SEM results in Fig. 3, it may be related with the enlarged surface area contributed from the SDC phase. However, the strong dependence of ASR on firing temperature suggests that the ASR could also be closely related with the phase reaction between BSCF and SDC.

As shown in Figs. 2–4, phase reaction between BSCF and SDC with the formation of new perovskite (Ba,Sr,Sm, Ce)(Co,Fe)$O_{3-\delta}$ could occur, depending on the firing temperatures. The electrical and electrochemical properties of

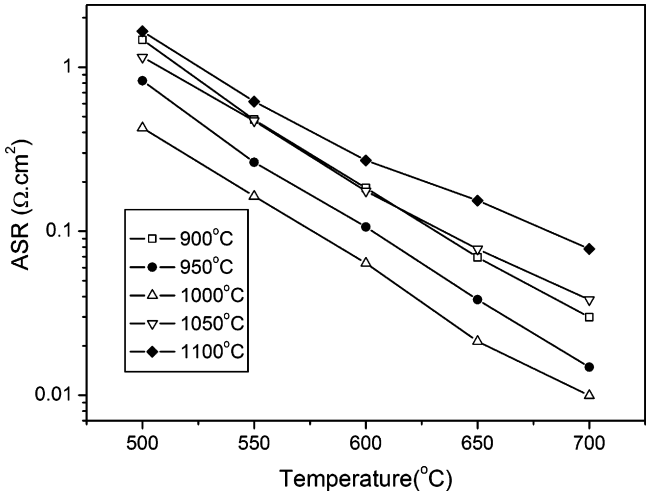

Fig. 5. Effect of firing temperature on the area specific resistance of BSCF + SDC (70:30 in weight ratio) electrode based on symmetric cell configuration.

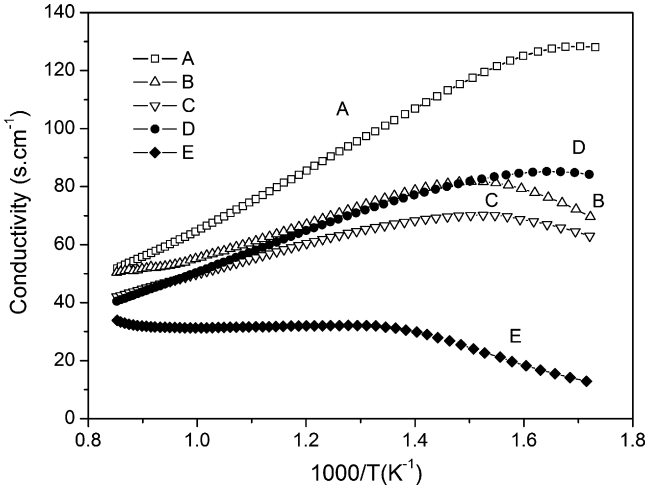

Fig. 6. Temperature dependence of electrical conductivities of (A) $Sm_{0.2}(Ba_{0.5}Sr_{0.5})_{0.8}Co_{0.8}Fe_{0.2}O_{3-\delta}$; (B) $Ce_{0.2}(Ba_{0.5}Sr_{0.5})_{0.8}Co_{0.8}Fe_{0.2}O_{3-\delta}$; (C) $(Sm_{0.2}Ce_{0.8})_{0.2}(Ba_{0.5}Sr_{0.5})_{0.8}Co_{0.8}Fe_{0.2}O_{3-\delta}$; (D) sol–gel derived BSCF + SDC composite; (E) $Ba_{0.5}Sr_{0.5}Co_{0.8}Fe_{0.2}O_{3-\delta}$.

the reaction products between BSCF and SDC were then investigated. Fig. 6 shows the electrical conductivity of the BSCF, sol–gel derived BSCF + SDC composite, A-site Sm^{3+} incorporated BSCF ($Sm_{0.2}Ba_{0.4}Sr_{0.4}Co_{0.8}Fe_{0.2}$ $O_{3-\delta}$), A-site Ce^{4+} incorporated BSCF ($Ce_{0.2}Ba_{0.4}Sr_{0.4}Co_{0.8}Fe_{0.2}O_{3-\delta}$), and A-site ceria and samaria incorporated BSCF ($(Sm_{0.2}Ce_{0.8})_{0.2}Ba_{0.4}Sr_{0.4}Co_{0.8}Fe_{0.2}O_{3-\delta}$), measured by four-terminal DC techniques. It shows that the doping of Sm^{3+} and Ce^{3+} into the A-site of BSCF perovskite resulted in the increased electrical conductivity of the oxide. Such improvement can be explained in part by the fact that the doping of Ce^{3+} and Sm^{3+} into A-site of the BSCF resulted in the shrinking of the lattice. Because Ce^{3+}/Sm^{3+} have smaller ionic size than Ba^{2+}/Sr^{2+}, their doping in the A-site of the BSCF promotes the B-site metal ions to take a higher valence state. Consequently, the distance between the B-site metals became closer and thus it is easier for electron exchange between the B-site ions to occur. On the other hand, Ce^{3+}/Sm^{3+} have a higher valence state than Ba^{2+}/Sr^{2+}, and thus the doping of Ce^{3+}/Sm^{3+} into the A-site of the BSCF reduced the oxygen vacancy concentration, which also is also beneficial for increasing the p-type conductivity. The electrode performances of sol–gel derived BSCF + SDC composite and $(Sm_{0.2}Ce_{0.8})_{0.2}Ba_{0.4}Sr_{0.4}$ $Co_{0.8}Fe_{0.2}O_{3-\delta}$, were measured based on symmetric cell configuration and a comparison with the pure BSCF cathode. The same firing temperature of 1000 °C was selected in this investigation to ensure similar cathode morphologies for all the samples. As shown in Fig. 7, both sol–gel derived BSCF + SDC and $(Sm_{0.2}Ce_{0.8})_{0.2}Ba_{0.4}$ $Sr_{0.4}Co_{0.8}Fe_{0.2}O_{3-\delta}$ demonstrated relatively worse cathode performance when compared with the BSCF. Such a decrease in electrode performance can be related to the reduced oxygen vacancy concentration due to the incorporation of Ce^{3+}/Sm^{3+} in the A-site of BSCF.

Based on above results, a reaction mechanism between the BSCF and SDC for the high-temperature firing and the influence of the reaction on the cathode performance of the composite

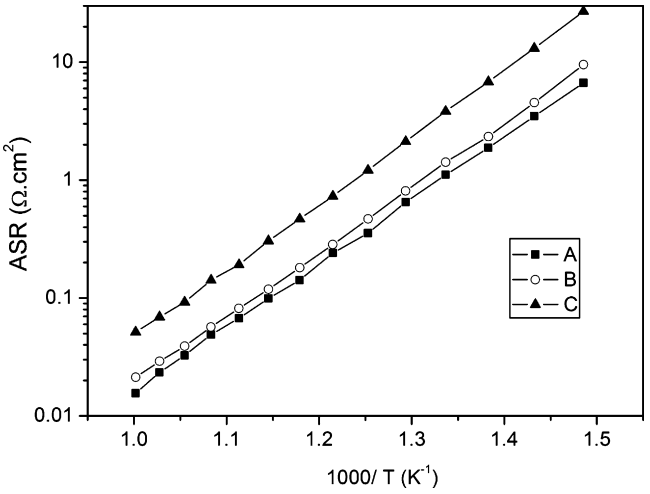

Fig. 7. Temperature dependence of ASRs (A) BSCF; (B) sol–gel derived BSCF + SDC composite; (C) $(Sm_{0.8}Ce_{0.2})_{0.2}(Ba_{0.5}Sr_{0.5})_{0.8}Co_{0.8}Fe_{0.2}O_{3-\delta}$.

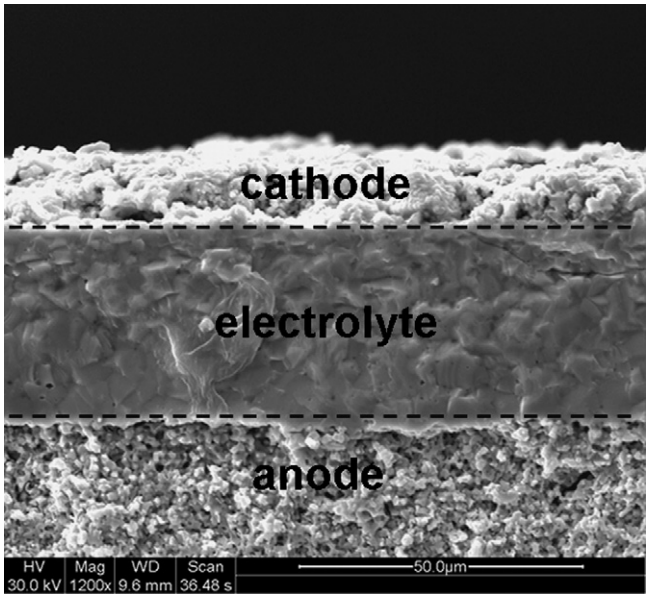

Fig. 9. A fraction surface micrograph of a single cell based on BSCF + SDC cathode and NiO + SDC anode and SDC electrolyte.

oxide, as shown in Fig. 8, was proposed. The mechanical mixing of the BSCF and SDC resulted in the fine SDC particles being loosely attached to the surfaces of the big BSCF grains. At a temperature of 900 °C, the reaction between the BSCF and SDC was negligible. However, the connection between the BSCF and SDC particles was also poor after firing at this temperature, which resulted in a relatively high interfacial polarization. Therefore, large ASRs were observed for the cathode fired at this temperature. The steady increase of firing temperature resulted in enhanced particle connections, which account for the improved ASRs with increasing temperature up to 1000 °C. When the firing/calcination temperature reached 1000 °C, the inter-diffusion between BSCF and SDC was enhanced and the constricted solid-state reaction between BSCF and SDC occurred with the formation of a third phase of $(Ba,Sr,Ce,Sm)(Co,Fe)O_{3-\delta}$ at their phase boundary. The limited reactive sintering aided in the adhesion of fine SDC particles to the BSCF surfaces firmly. In connection with the higher electronic conductivity of the third phase than with the reactants of BSCF and SDC, an improved current distribution efficiency could then be expected, which is beneficial for reducing the interfacial polarization resistance. Although the new phase has worse activity for oxygen reduction than the BSCF, its detrimental effect on the cathode performance is negligible since it located only along the BSCF and SDC interface and its thickness is small due to the limited reaction. Instead, the relatively higher surface area of the SDC phase successfully enlarged the active sites for oxygen reduction. In connection with the good electrochemical activity of SDC for oxygen adsorption and activation, the improved cathode performance of the BSCF + SDC composite cathode fired at 1000 °C as compared with the pure BSCF cathode, is then well understood. With the further increase of the firing temperature to 1050 °C or higher, however, the diffusion block between the BSCF and SDC phases was successfully overcome, which resulted in the formation of the $(Ba,Sr,Sm,Ce)(Co,Fe)O_{3-\delta}$ new phase throughout the entire cathode, a material with worse cathode performance than BSCF. Furthermore, the cathode sintering was also accelerated. Both detrimental effects resulted in a sharp decrease in cathode performance with the further increase of the firing temperature.

Finally, an optimal firing temperature of 1000 °C for fabricating the BSCF + SDC cathode layer was developed. Whole

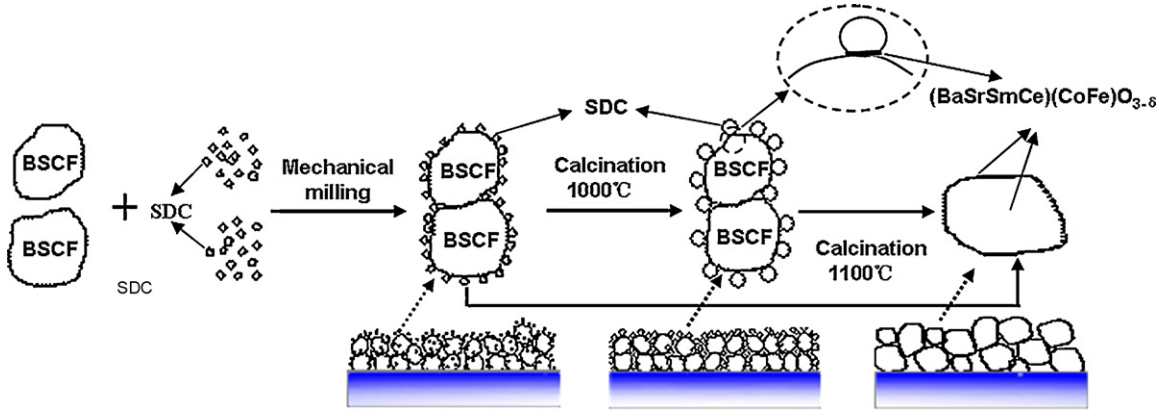

Fig. 8. Diagram for the sintering mechanism of BSCF + SDC composite cathode.

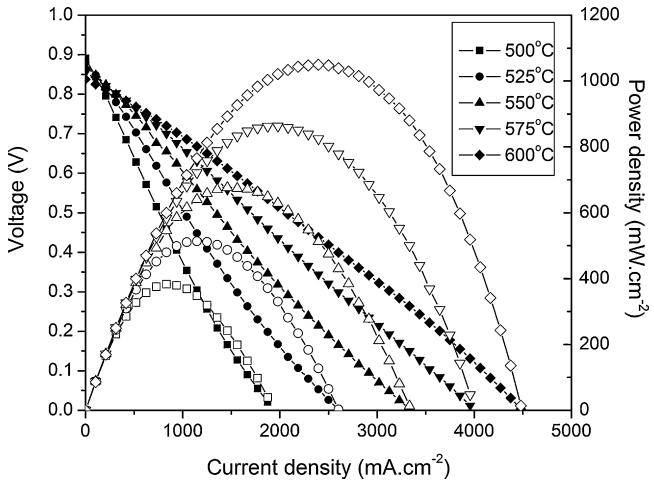

Fig. 10. The dependence of cell voltages and power densities on current densities of cell tested at various temperature between 500 and 600 °C.

cells with the BSCF + SDC cathode fired from 1000 °C were then fabricated for further fuel cell performance tests. Fig. 9 shows the typical SEM micrograph of the fractured surfaces of an anode-supported fuel cell. The fuel cell was composed of an Ni + SDC anode with a thickness of ∼0.5 mm, SDC electrolyte of ∼30 μm, and BSCF + SDC cathode of 10 μm. Shown in Fig. 10 is the dependence of cell voltages and power densities on current densities of the cell tested at various temperatures between 500 and 600 °C with similar cell configuration as shown in Fig. 9. Ambient air was applied as the cathode atmosphere and pure hydrogen as the fuel during the study. A maximum peak power density of 1050 mW cm^{-2} was achieved at 600 °C with the open circuit voltage of ∼0.84 V, which are comparable or even slightly better than results from the similar fuel cell based on the pure BSCF cathode [16]. At 500 °C, a promising peak power density of ∼382 mW cm^{-2} was still reached. Shown in Fig. 11 are the electrochemical impedance spectra of the cell under OCV condition. It was mainly composed of two parts. The left arc (high frequency) is contributed of ohmic polarization, including the effective resistance between cathode and anode, the ohmic resistance of the connection leads, while the right arc (low frequency) is due to the total polarization resistance of electrodes including anode and cathode. An electrode resistance of only 0.048 and 0.25 Ω cm^2 was observed at 600 and 500 °C, respectively, which are even smaller than the corresponding ASRs of the BSCF + SDC based on the symmetric cell configuration. This suggests that the cathode performance was even improved under the asymmetric cell condition on the one hand and negligible anode polarization on the other hand.

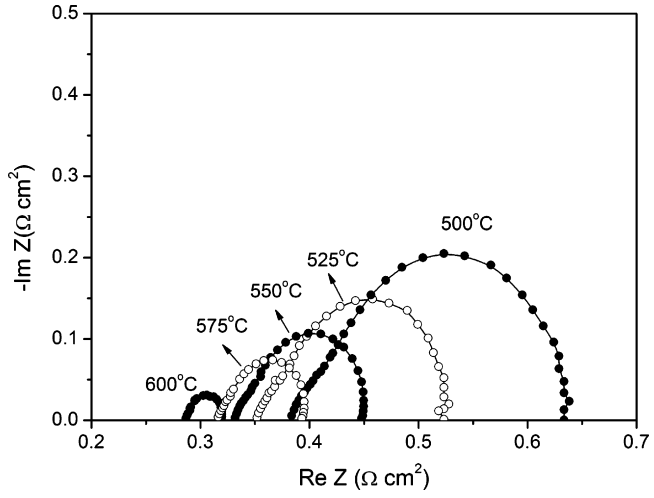

Fig. 11. Impedance spectroscopies of the anode-supported fuel cell with 1000 °C calcined BSCF + SDC (70:30 in weight ratio) at various temperatures under OCV conditions.

4. Conclusions

Based on the above results the following conclusions could be made. The solid-state reaction between BSCF and SDC in the BSCF + SDC (70:30 in weight ratio) composite cathode is greatly contingent on the firing temperature. At 900 °C or lower, negligible reaction occurred. At ∼1000 °C, the reaction occurred at the BSCF + SDC interface only, with the formation of the third phase of (Ba,Sr,Ce,Sm)(Co,Fe)$O_{3-\delta}$ perovskite from the incorporation of Sm^{3+} and Ce^{3+} into the A-site of BSCF. When the firing temperature was elevated to ∼1050 °C or higher, the reaction progressed throughout the entire cathode with the formation of (Ba,Sr,Ce,Sm)(Co,Fe)$O_{3-\delta}$ perovskite, which had higher electronic conductivity than BSCF but worse activity for oxygen reduction due to the decrease in lattice size and oxygen vacancy concentration. Therefore, obvious increase of polarization resistance for oxygen reduction was observed when BSCF + SDC was fired at ∼1100 °C. At a modest firing temperature of 1000 °C, the reaction occurred only at the interface of BSCF and SDC, which did not produce a detrimental effect on the oxygen reduction process; on the contrary, it resulted in good connection between the BSCF and SDC particles in the BSCF + SDC composite cathode and helped to reduce the interfacial resistance. Furthermore, the SDC enlarged the effective cathode surface area due to the higher surface area of SDC in comparison to BSCF. Therefore, an improved cathode performance was observed for the 1000 °C calcined BSCF + SDC composite cathode as compared to the pure phase BSCF. Complete fuel cells with the BSCF + SDC cathode fired from 1000 °C were then fabricated. A peak power density as high as 1050 mW cm^{-2} was achieved at 600 °C.

Acknowledgements

This work was supported by the National Natural Science Foundation of China, under contracts: No. 20646002, and 20676061, and National Basic Research Program of China under contract No. 2007CB209704.

References

[1] B.C.H. Steele, P.H. Middleton, R.A. Rudkin, Solid State Ionics 40/41 (1990) 388–393.
[2] E.P. Murray, T. Tsai, S.A. Barnett, Nature 400 (1999) 649–651.
[3] S. Park, J.M. Vohs, R.J. Gorte, Nature 404 (2000) 265–267.
[4] O. Yamamoto, Y. Takeda, R. Kanno, M. Noda, Solid State Ionics 22 (1987) 241–246.

[5] H.Y. Tu, Y. Takeda, N. Imanishi, O. Yamamoto, Solid State Ionics 117 (1999) 277–281.
[6] A. Mitterdorfer, L.J. Gauckler, Solid State Ionics 111 (1998) 185–218.
[7] J.Y. Yi, G.M. Choi, J. Eur. Ceram. Soc. 24 (2004) 1359–1363.
[8] N.Q. Minh, J. Am. Ceram. Soc. 76 (1993) 563–588.
[9] X.G. Zhang, M. Robertson, S. Yick, C. Deces-Petit, E. Styles, W. Qu, Y.S. Xie, R. Hui, J. Roller, O. Kesler, R. Maric, D. Ghosh, J. Power Sources 160 (2006) 1211–1216.
[10] S.Z. Wang, Y.M. Zou, Electrochem. Commun. 8 (2006) 927–931.
[11] R. Pelosato, I.N. Sora, G. Dotelli, R. Ruffo, C.M. Mari, J. Eur. Ceram. Soc. 25 (2005) 2587–2591.
[12] T. Suzuki, M. Awano, P. Jasinski, V. Petrovsky, H.U. Anderson, Solid State Ionics 177 (2006) 2071–2074.
[13] A. Esquirol, J. Kilner, N. Brandon, Solid State Ionics 175 (2004) 63–67.
[14] S.Y. Li, Z. Lü, B. Wei, X.Q. Huang, J.P. Miao, Z.G. Liu, W.H. Su, J. Alloys Compd. 448 (2008) 116–121.
[15] Q.S. Zhu, T.A. Jin, Y. Wang, Solid State Ionics 177 (2006) 1199–1204.
[16] Z.P. Shao, S.M. Haile, Nature 431 (2004) 170–173.
[17] J. Peña-Martínez, D. Marrero-López, J.C. Ruiz-Morales, B.E. Buergler, P. Núñez, L.J. Gauckler, Solid State Ionics 177 (2006) 2143–2147.
[18] Y.H. Lim, J. Lee, J.S. Yoon, C.E. Kim, H.J. Hwang, J. Power Sources 171 (2007) 79–85.
[19] Q.L. Liu, K.A. Khor, S.H. Chan, J. Power Sources 161 (2006) 123–128.
[20] Z.P. Shao, S.M. Haile, J. Ahn, P.D. Ronney, Z. Zhan, S.A. Barnett, Nature 435 (2005) 795–798.
[21] K. Wang, R. Ran, Z.P. Shao, J. Power Sources 170 (2007) 251–258.
[22] Z.P. Shao, J. Mederos, W.C. Chueh, S.M. Haile, J. Power Sources 162 (2006) 589–596.
[23] W. Zhou, Z.P. Shao, W.Q. Jin, J. Alloys Compds. 426 (2006) 368–374.
[24] N.E. Trofimenko, H. Ullmann, J. Eur. Ceram. Soc. 20 (2000) 1241–1250.
[25] N.E. Trofimenko, J. Paulsen, H. Ullmann, R. Muller, Solid State Ionics 100 (1997) 183–191.
[26] S.Y. Li, Z. Lu, X.Q. Huang, B. Wei, W.H. Su, Solid State Ionics 178 (2007) 417–422.
[27] J. Peña-Martínez, D. Marrero-López, D. Pérez-Coll, J.C. Ruiz-Morales, P. Núñez, Electrochim. Acta 52 (2007) 2950–2958.
[28] Y. Sakaki, Y. Takeda, A. Kato, N. Imanishi, O. Yamamoto, M. Hattori, M. Iio, Y. Esaki, Solid State Ionics 118 (1999) 187–194.
[29] S.Y. Li, Z. Lu, N. Ai, K.F. Chen, W.H. Su, J. Power Sources 426 (2006) 408–414.
[30] W. Zhou, Z.P. Shao, R. Ran, P.Y. Zeng, H.X. Gu, W.Q. Jin, N.P. Xu, J. Power Sources 168 (2007) 330–337.
[31] C.R. Xia, W. Rauch, F.L. Chen, M.L. Liu, Solid State Ionics 149 (2002) 11–19.
[32] E.P. Murray, S.A. Barnett, Solid State Ionics 143 (2001) 265–273.
[33] E.P. Murray, M.J. Sever, S.A. Barnett, Solid State Ionics 148 (2002) 27–34.